Flexural Behaviour of Headed Bar Connections between Precast Concrete Panels

Jean Paul Vella[a], Robert L. Vollum[a], Andrew Jackson[b]

[a]Department of Civil and Environmental Engineering, Imperial College London, London, UK

[b]Engineering Excellence Group, Laing O'Rourke, Dartford, UK

Abstract

The use of headed bars in joints between precast concrete elements allows continuity of reinforcement to be achieved over very short splice lengths. The paper describes a series of flexural tests carried out on specimens consisting of pairs of precast elements connected by overlapping headed bars of 25 mm diameter. The headed bars overlapped by 100 mm within a 200 mm wide insitu concrete joint in which transverse bars and vertical shear studs were installed to provide confinement. This type of joint facilitates the construction of continuously reinforced slabs from precast elements thereby enabling significant reductions in overall construction time and improvements in construction quality due to off-site fabrication. The tests investigated the influence on joint strength, ductility and crack width of concrete strength, out-of-plane offset of precast planks and confining shear studs. Ductile failure with yield of 25 mm diameter high strength headed bars was achieved with joint concrete having a cylinder compressive strength of 39 MPa. A nonlinear finite element model is presented, which gives good predictions of joint strength as well as providing insight into joint behaviour.

Keywords: Precast concrete, Headed reinforcement, Lap length, Strut-and-tie, Nonlinear finite element analysis.

Notation

ε_2	NLFEA reinforcement strain at end of yield/start of strain hardening
ε_3	NLFEA reinforcement ultimate strain
ε_c	Strain in the compression zone concrete
ε_{c1}	Strain at peak compressive stress
ε_s	Shear stud measured strain
η	Concrete strain ratio
σ_2	NLFEA reinforcement stress at end of yield/start of strain hardening
σ_3	NLFEA reinforcement ultimate stress
σ_c	Concrete compressive stress
σ_y	NLFEA steel yield stress
υ	NLFEA steel Poisson's ratio
$\emptyset_b$	Reinforcement diameter
$\emptyset_{tr}$	Transverse bar diameter
E_{cm}	Concrete elastic modulus
E_s	Reinforcement elastic modulus
H	NLFEA steel hardening modulus
L_{hb}	Headed bar lap length between bearing faces of heads
M	Maximum moment at joint-precast interface
M_{hb}	Bending moment at bar head
M_{fl}	Maximum applied bending moment at joint-precast interface
$M_{p,hb}$	Longitudinal headed bar plastic moment resistance
$M_{p,tr}$	Transverse bar plastic moment resistance
M_{test}	Maximum measured or equivalent calculated bending moment achieved in test
M_{tr}	Bending moment in transverse bar
N_{hb}	Measured longitudinal headed bar force
N_{2hb}	Longitudinal headed bar force on the two bar side
$N_{3hb,centre}$	Central longitudinal headed bar force on the three bar side
$N_{3hb,edge}$	Edge longitudinal headed bar force on the three bar side
$N_{y,hb}$	Longitudinal headed bar yield load

$N_{y,tr}$	Transverse bar yield load
N_{tr}	Force in transverse bar
N_s	Force in shear stud
P	Maximum flexural test load
P_{tens}	Maximum tensile test measured load
P_{fl}	Maximum flexural test measured load
S_{hb}	Spacing of headed bars with same orientation
S_F	Shear factor in NLFEA
d_g	Maximum aggregate size in NLFEA
f'_c	NLFEA concrete cylinder compressive strength
f'_{c0}	Onset of nonlinear behaviour in NLFEA
f'_t	NLFEA concrete tensile strength
$f_{c,cyl,j}$	Measured joint concrete cylinder compressive strength
$f_{c,cyl,p}$	Measured precast concrete cylinder compressive strength
f_{cm}	Mean concrete cylinder compressive strength
$f_{ct,j}$	Measured joint concrete tensile strength
f_u	Reinforcement ultimate strength
f_y	Reinforcement yield strength
r_c	Compressive strength of cracked concrete factor in NLFEA
w_d	Plastic displacement in concrete softening law in NLFEA
x_2	Precast slab out-of-plane offset
x_t	Transverse bar offset from the centreline of the joint

1. Introduction

The paper investigates the performance of narrow cast in-situ joints between precast concrete elements in which continuity of reinforcement is achieved through overlapping headed bars, as shown in Figure 1. Using headed instead of straight bars, significantly reduces tension splice lengths, thereby facilitating very efficient construction systems, like the 'E6 floor system' patented by Laing O'Rourke, in which headed bar splices provide continuity between precast elements within the floor depth. The narrow joint width adopted in the E6 system, made possible by the use of headed bars, allows adjacent precast units to be supported off each other during construction with easily handled steel brackets. This significantly reduces traditional propping, thereby enabling other follow-on trades to commence earlier. This in turn reduces overall construction time and improves on-site health and safety as well as construction quality due to trades being moved offsite into the factory. The system is ideal for regular slab layouts with standardised components, but can accommodate bespoke floor arrangements.

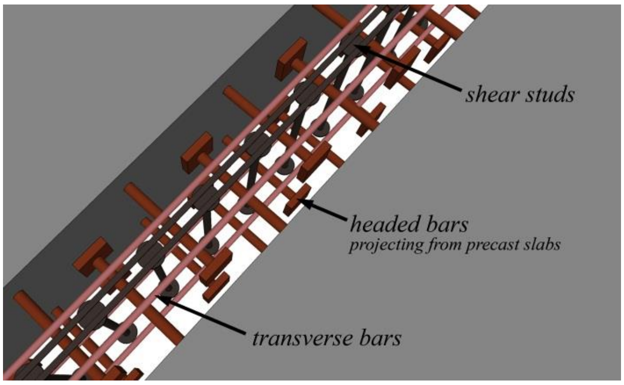

Figure 1: Typical headed bar joint

Similar connections using lapped headed bars, but with smaller diameter bars or longer laps, and U-bars have been studied by other researchers with the main emphasis on bridge deck applications [1-13]. A variety of design approaches have been proposed for these joints, including: models based on the ACI 318-02 [14] recommendations for side-blowout and bearing strength, strut-and-tie models [4, 9-11], and an upper bound plasticity based model [12, 13]. The authors have previously tested a series of tension specimens with the geometry shown in Figure 2 which is intended to simulate a headed bar splice within the tension zone of a 300 mm thick slab loaded in flexure. The tension tests investigated the influence of variables including concrete strength, transverse reinforcement area and arrangement and presence or absence of confining shear studs [15].

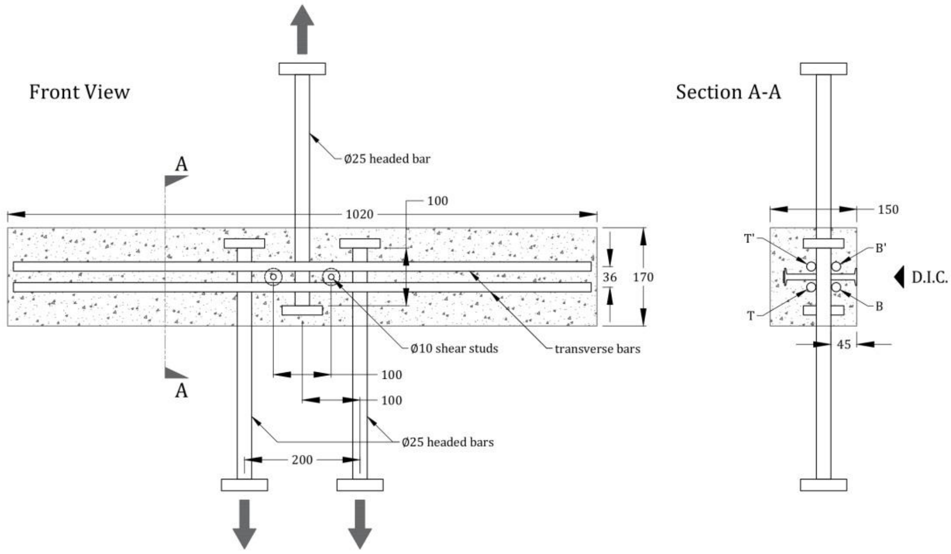

Figure 2: Typical tensile test specimen

This paper describes a series of five flexural tests which were carried out to investigate the influence on joint strength of concrete strength, out-of-plane offset of precast slabs and confining shear studs. The bar heads used in the tension and flexural tests were sufficiently large to develop the full tensile strength of the bars without any contribution from bond [16]. Therefore, tension is mainly transferred between overlapping headed bars through a series of diagonal compressive struts as shown in Figure 3 in which the the transverse headed bars resist out of balance forces at ends of diagonal struts. The paper compares and contrasts the behaviour of the headed bar splice joints in the authors' tension and flexural tests.

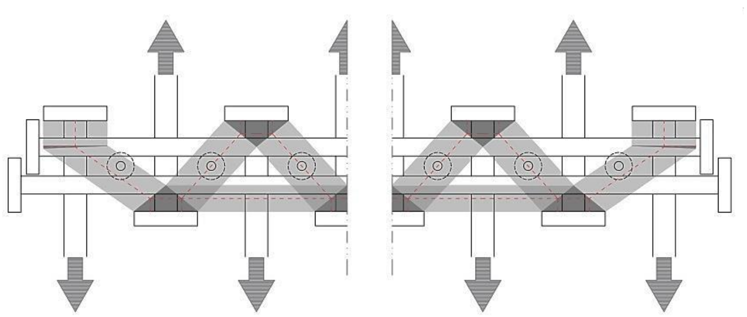

Figure 3: Tensile force transfer within headed bar joint (plan)

2. Laboratory Testing

2.1. Tension Test Specimen Details

A full description of the direct tension tests is given elsewhere [15] so only pertinent points are summarised here. In total 27 tension specimens were tested to investigate the influence on joint strength of variables including concrete strength, transverse reinforcement and presence or absence of confining shear studs. The headed bars used in the tests were 25 mm in diameter with 70 mm square heads and yield strength of 530 MPa. Only specimens G1-26-2H20:TT'-S-100-200, G1-40-2H20:TT'-S-100-200 and G2-26-2H20:TT'-100-200 are discussed in this paper since they are directly comparable with flexural tests B2-26-2H20-S-0, B2-39-2H20-S-0 and B2-24-2H20-/-0 respectively. The geometrical dimensions and longitudinal reinforcement arrangement of these specimens (see Figure 2) are the same as for the uncracked tension zone of the tested slabs. Where present, two 10 mm diameter 125 mm long shear studs with 30 mm diameter heads were placed in the positions shown in Figure 2. The minimum and maximum covers to the stud head were zero and 25 mm. The 36 mm spacing of the transverse bars shown in Figure 2 was chosen to allow sufficient space for concrete to be placed in contact with the bar heads and to allow clearance for the friction weld flash. The tests focussed on concrete controlled failures with a view to determining the critical concrete strength at which bar yield precedes concrete failure. Table 1 provides details of the three tension specimens most pertinent to this study. The test ID describes the specimens as follows:

For example, G1-26-2H20:TT'-S-100-200:

" G1 " – Test group
" 26 " – Measured concrete cylinder strength at time of testing
" 2H20 " – Number and diameter of transverse bars
" TT' " – Position of transverse bars as indicated in Figure 2
" S " – Shear studs included
" 100 " – Lap length of headed bars
" 200 " – Spacing of headed bars

In Table 1, $f_{c,cyl,j}$ and $f_{ct,j}$ are the measured concrete cylinder compressive strength and tensile splitting strength respectively. $Ø_{tr}$ is the transverse bar size, S_{hb} is the spacing of the headed bars in the same orientation, L_{hb} is the lap length between the bearing faces of the heads and x_t is the offset of the transverse bars from the centreline of the joint. P_{tens} is the maximum load achieved in each test. For reference, the headed bar yield load was 260 kN. The response of the three tension specimens in Table 1 is discussed later alongside that of the relevant slab tests.

Test ID	$f_{c,cyl,j}$ (MPa)	$f_{ct,j}$ (MPa)	$\emptyset_{tr}$ (mm)	Transverse Bar Positions	S_{hb} (mm)	L_{hb} (mm)	x_t (mm)	P_{tens} (kN)
G1-26-2H20:TT'-S-100-200	25.6	2.38	20	T T'	200	100	18	154
G1-40-2H20:TT'-S-100-200	40.4	3.60	20	T T'	200	100	18	242
G2-26-2H20:TT'-100-200	25.6	2.38	20	T T'	200	100	18	133

Table 1: Tension test specimen details

2.2. Flexural Test Specimen Details

Five flexural specimens were tested of which one was a control specimen. A symmetrical five bar reinforcement arrangement was chosen in preference to an unsymmetrical six bar arrangement to avoid inducing secondary in-plane rotational stresses of the type observed by Gordon and May [7].

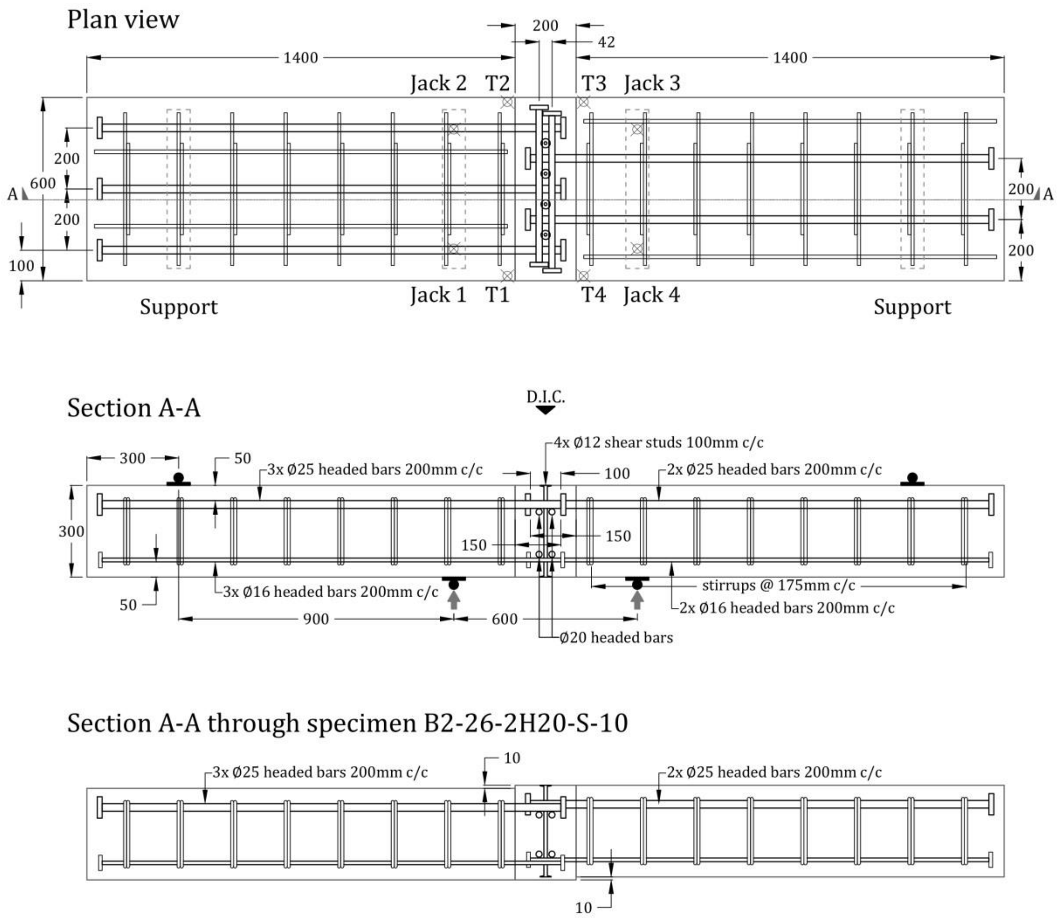

Figure 4: Typical flexural test specimen and section through specimen B2-26-2H20-S-10

The headed longitudinal bars were spaced at 200 mm centres with a 100 mm lap length between the inside face of the heads as used in the standard arrangement of the Laing O'Rourke E6 system. 50 mm cover was provided to the main bars in both layers. The tested variables were joint concrete strength, the presence or absence of shear studs and out-of-plane offset of the precast planks. The headed bars in the tensile zone were 25 mm in diameter with standard 70 x 70 x 16 mm friction welded square heads. The diameter of the headed bars near the compression zone was 16 mm, with standard 50 x 50 x 12 mm friction welded square heads. Two 20 mm transverse headed bars with 60 x 60 x 14 mm friction welded square heads were provided on the inside face of each layer of longitudinal reinforcement as shown in Figure 4. The spacing between the centrelines of the transverse bars of 42 mm is the minimum allowed by the head size, including some tolerance. Where present, four 12 mm diameter shear studs were provided in the positions shown in Figure 4. The shear studs were 300 mm long leaving no cover to the heads which were 36 mm in diameter. Specimens were cast in timber moulds with the joint faces of the precast sections left as cast and wetted lightly before the joint concrete was cast. The control specimen was continuously reinforced as in the right hand precast unit of Figure 4. The end sections of the control specimen were cast before the central 200 mm joint to isolate the influence of reinforcement detailing on joint behaviour. In all cases, the joint was cast at least three weeks after the precast sections. Table 2 summarises the details of the tested specimens, with the test ID describing specimens as follows:

For example, B2-39-2H20-S-0:

" B2 " – Test group

" 39 " – Measured joint concrete cylinder strength at time of testing

" 2H20 " – Number and diameter of transverse bars

" S " – Shear studs included

" 0 " – Out-of-plane offset of precast planks

Specimens B2-26-2H20-S-0 and B2-39-2H20-S-0 investigated the influence on joint strength of concrete strength, while specimens B2-24-2H20-/-0 and B2-26-2H20-S-10 respectively investigated the influence of shear studs and out-of-plane offset of the precast planks. The offset was achieved by lowering the three bar precast unit by 10 mm relative to the two bar unit and the joint infill was cast over the full depth of 310 mm as shown in Figure 4. In this case, zero cover was provided to the shear stud in the tensile zone. The precast planks used in specimen B2-24-2H20-/-0 were reclaimed from specimen B2-26-2H20-S-0 after testing the joint to failure.

Concrete compressive and tensile strengths were measured from control specimens cured in the same conditions and tested at the same time as the slabs. 100 mm diameter, 200 mm high cylinders were used to determine compressive strength according to BS EN 12390-3:2009 [17] for both joint and precast concrete. Joint concrete tensile strength was determined by means of splitting tests according to BS EN 12390-6:2009 [18] on 300 mm high cylinders with a diameter of 150 mm. At least three specimens of each type were tested. The resulting concrete strengths are given in Table 2 which also gives geometrical details and failure loads of the slabs. In Table 2, $f_{c,cyl,p}$, $f_{c,cyl,j}$ and $f_{ct,j}$ are the measured precast slab concrete cylinder compressive strength, joint concrete cylinder compressive strength and joint concrete tensile splitting strength respectively, and x_2 is the out-of-plane offset of the precast planks.

Test ID	$f_{c,cyl,p}$ (MPa)	$f_{c,cyl,j}$ (MPa)	$f_{ct,j}$ (MPa)	$\varnothing_{tr}$ (mm)	S_{hb} (mm)	L_{hb} (mm)	x_t (mm)	x_2 (mm)	P_{fl} (kN)	M_{fl} (kNm)
B1-39-/-/-/	65.2	39.3	3.40	—	—	—	—	0	362	160
B2-26-2H20-S-0	60.4	25.7	2.46	20	200	100	21	0	253	111
B2-39-2H20-S-0	65.2	39.3	3.40	20	200	100	21	0	293	129
B2-24-2H20-/-0	N/A	24.1	2.58	20	200	100	21	0	192	84
B2-26-2H20-S-10	60.4	25.7	2.46	20	200	100	21	10	225	99

Table 2: Flexural test specimen details

Reinforcement material properties were derived from coupon tension tests according to BS EN ISO 6892-1:2009 [19]. Three specimens of each bar type were tested with average results of the main reinforcement given in Table 3. Figure 5 shows stress-strain curves for the 25mm headed bar coupon tests wherein strains were measured with strain gauges and stresses calculated considering a cross-sectional bar area of 490.9 mm^2.

Type	$\varnothing_b$ (mm)	Head size (mm)	f_y (MPa)	f_u (MPa)	E_s (GPa)
Headed bar	25	70 x 70 x 16	530	636	197
Headed bar	20	60 x 60 x 14	516	631	201
Shear stud	12	Ø36	564	656	223

Table 3: Flexural test specimen reinforcement properties

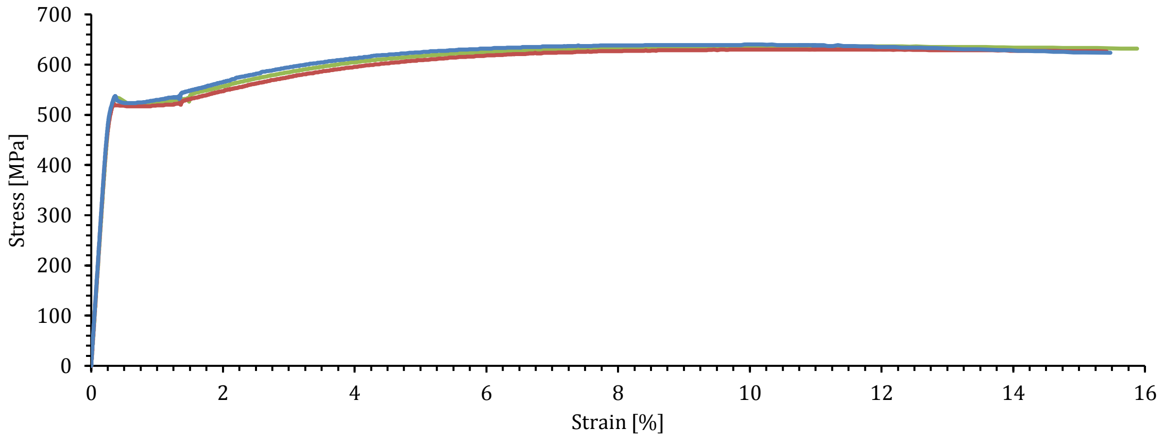

Figure 5: Stress-strain curves for 25 mm headed bar coupon tests

2.3. *Test Setup and Instrumentation*

The slabs were loaded in four point bending from their underside to enable digital image correlation (DIC) to be used to monitor cracking in the tension face (see Figure 4 Section A-A). The spans between centrelines of supports and loading points were 2400 mm and 600 mm respectively (see Figure 6). The slabs were loaded across their width through a pair of 75 mm wide, 10 mm thick solid steel rectangular sections. End supports were provided by stiff built-up steel sections anchored to the laboratory strong floor as shown in Figure 6. 30 mm diameter roller bearings were provided at the end supports of the slab to release horizontal translation and rotation arising from curvature of the beam upon loading. Loads were applied with two pairs of hydraulic actuators fed by a single inlet to maintain equal pressure.

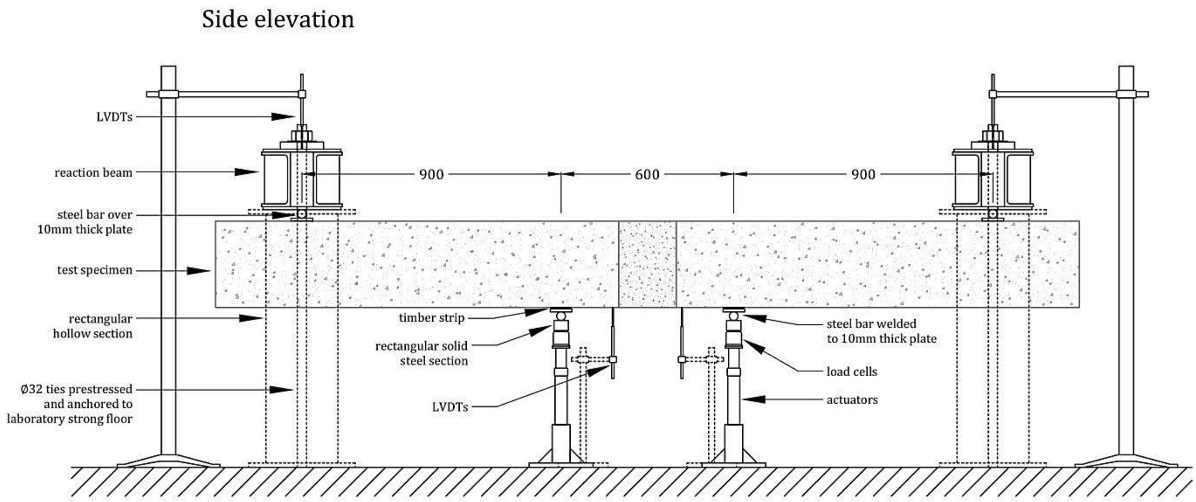

Figure 6: Flexural test rig

Loads were measured with load cells placed at each actuator. Displacements were measured with two pairs of linear variable displacement transducers (LVDTs) placed near the precast-to-joint interfaces as shown in Figure 6, along with an additional pair at each support to determine any global movement of the specimen during loading. Strain gauges were fixed to the reinforcement inside the joint of headed bar specimens as shown in Figure 7a, with the aim of capturing both bending and axial forces. Pairs of gauges were mounted diametrically opposite each other in either horizontal (e.g. S9-S10) or vertical (e.g. S1-S2) planes as shown in Figure 7a. Not all specimens were fully gauged, and specimen B2-24-2H20-/-0 was not gauged at all. Figure 7b also shows the positions of transverse bar strain gauges in the tensile specimens pertinent to this paper.

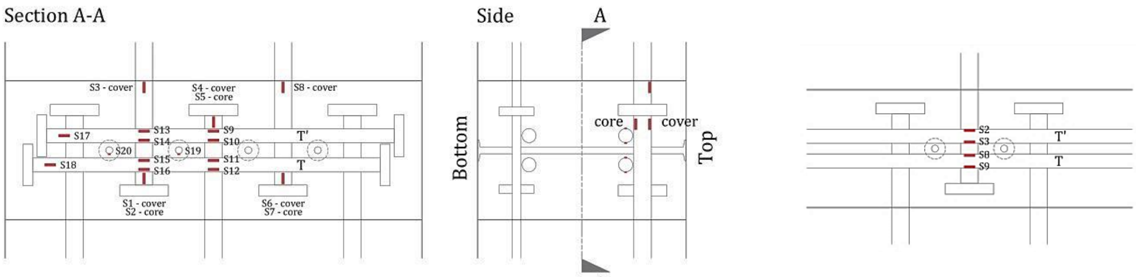

(a) (b)

Figure 7: Strain gauge positions in flexural specimens (a) and tension specimens (b)

A random speckle pattern was sprayed onto the surface of the specimen over the constant moment region to enable the LaVision StrainMaster system [20] to track the movement of the pattern by comparing images captured by the DIC cameras. Two high resolution cameras captured images of the surface of the specimen in stereo mode every 3 seconds. Since two cameras were used, it was possible to capture 3D displacements, surface strains and crack propagation.

3. Test Results and Observations

3.1. Strength and load-deflection response

For ease of reference, the slab response is henceforth related to the applied bending moment, including self-weight, at the precast to joint interface. The failure loads of the tested slabs are listed in Table 2 in which P_{fl} and M_{fl} respectively are the maximum applied load, including self-weight of around 13.5 kN, and corresponding bending moment. Load-deflection curves are presented in Figure 8. The load-deflection responses of the control specimen B1-39-/-/-/, with continuous reinforcement through the joint, and B2-39-2H20-S-0 are very similar up to near yield of the latter. The flexural reinforcement yielded on the two bar side of the joint-to-precast interface in B1-39-/-/-/and B2-39-2H20-S-0 at bending moments of 142 kNm and 118 kNm respectively. The greater resistance of B1-39-/-/-/ was due to the additional two 10 mm bars provided within the joint. Both specimens failed at large displacements, after extensive yielding of reinforcement, due to concrete crushing in the flexural compression zone within and adjacent to the joint. In the case of B2-39-2H20-S-0, concrete crushing also occurred in the joint around the headed bars loaded in tension.

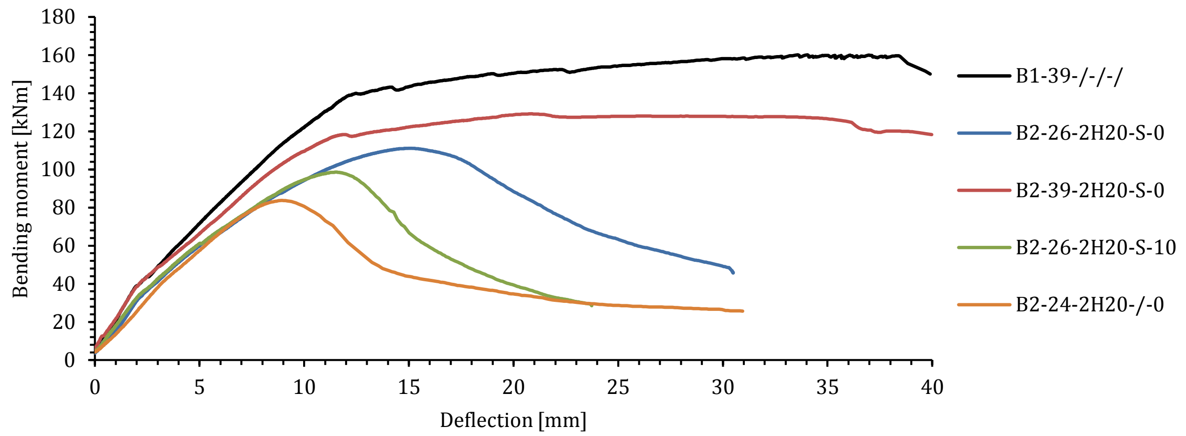

Figure 8: Load-deflection curves

The remaining specimens with lower joint concrete strengths of around 25 MPa failed within the joint prior to headed bar yield. Before failure, deflections of the lower concrete strength specimens were very similar and greater than that of B2-39-2H20-S-0 due to increased deformation within the joint. The post-peak load deflection curves of specimens with around 25 MPa concrete exhibit softening but also considerable ductility, unlike failure of straight bar splices which tends to be brittle. Offsetting the precast concrete planks in B2-26-2H20-S-10 out-of-plane by 10 mm reduced strength by 11%, but not stiffness, compared with B2-26-2H20-S-0. Specimen B2-24-2H20-/-0, without shear studs, achieved a peak moment around 24% less than that its companion specimen with shear studs, possibly due to loss of restraint to prying action resulting from curvature of the beam, as described by Chun [1].

3.2. Crack development and failure mechanism

DIC was used to continuously monitor crack development and surface principal strains. Figure 9 shows surface principal tensile strains in specimen B2-26-2H20-S-0 alongside comparable strains from NLFEA which are discussed subsequently. Strains are shown at the measured and predicted failure loads which correspond to bending moments at the precast to joint interface of 111 kNm and 95 kNm respectively. The magnitude of strain calculated with DIC is dependent on the size in pixels of a user defined subset within which the speckle pattern is monitored and correlated between images. The subset size was chosen such that the DIC strain was calculated over a gauge length of approximately 5 mm as in the NLFEA. Regions of high strain in Figure 9 correspond to cracks. Figure 10 shows the crack pattern at failure for the same specimen, which is typical. The first cracks to appear were transverse flexural cracks at the precast-to-joint interfaces, starting with crack 1 at the two bar interface (right hand side interface in Figure 4) at an applied bending moment of around 11 kNm. The longitudinal cracks 3 and 4 along the two headed bars propagated from the interface at a moment of 31 kNm. Crack 5 initiated near the two heads of the main bars at a moment of 45 kNm and subsequently extended towards the slab centreline and edges. Crack 6 near the head of the central headed bar appeared at a bending moment of 63 kNm, followed by cracks 7 and 8. Cracks 9 and 10 formed at bending moments of 70 kNm and 100 kNm respectively, followed by additional cracking close to the failure moment of 111 kNm.

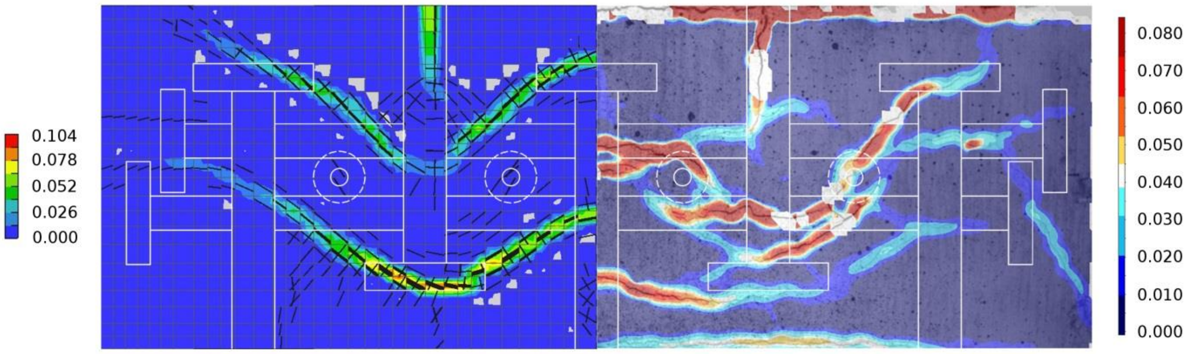

Figure 9: NLFEA (left) and test (right) crack pattern and maximum principal surface strain comparison for specimen B2-26-2H20-S-0

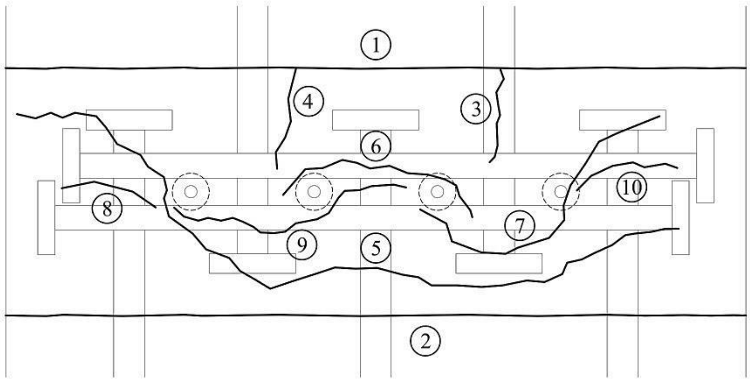

Figure 10: Specimen B2-26-2H20-S-0 schematic crack pattern

Figure 11a and Figure 11b respectively show the development of crack widths over the H25 headed bars on the two and three bar side of the joint. The applied load is shown as a proportion of the least of the measured yield and failure loads. The yield loads of B1-39-/-/-/ and B2-39-2H20-S-0 are estimated from Figure 8 to be 142 kNm and 118 kNm. All other specimens failed before reinforcement yield. Crack widths are greatest on the two bar side (Figure 11a) as expected except for B2-26-2H20-S-10 with 10 mm offset. EC2 [21] calculates crack widths under the quasi permanent load which for slabs is typically around 50% of the measured yield load assuming a partial factor of 1.15 for reinforcement. For concrete controlled failures, the ratio of quasi permanent to measured failure load is at most 40% assuming a partial factor for concrete of 1.5. For these load ratios, interface crack widths in Figure 11a and Figure 11b are at most

0.40 mm. Consequently, design crack widths under quasi permanent load are considered acceptable at the joint-to-precast interfaces.

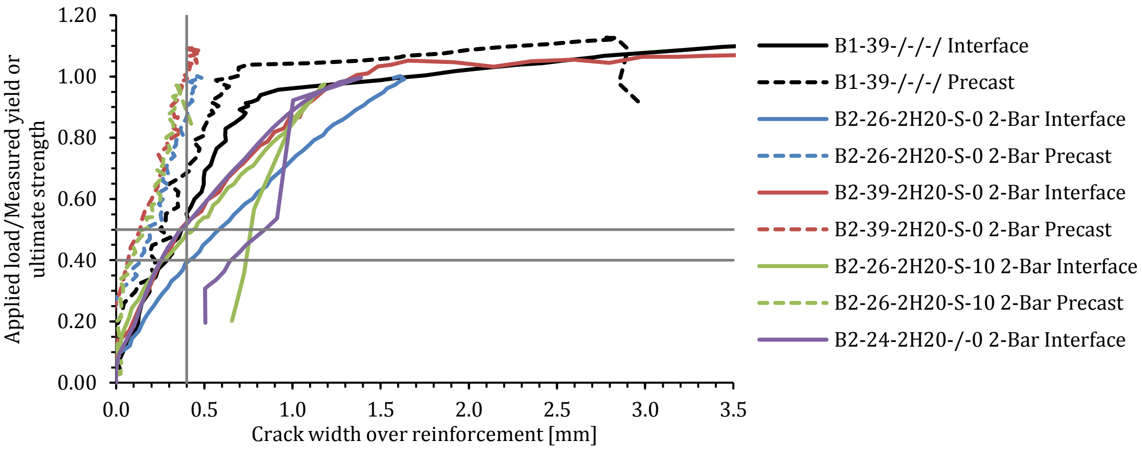

(a)

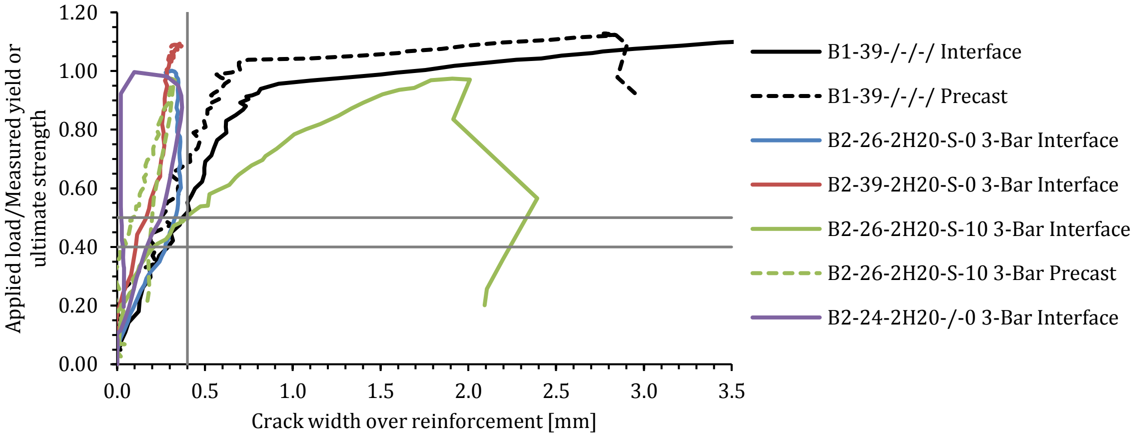

(b)

Figure 11: Crack widths versus load on a) two bar side and b) over centre bar of three bar side

Figure 12a and Figure 12b respectively show crack widths, at intervals of 100 mm, measured at the joint-to-precast interface crossed by two and three main bars respectively. Comparative crack widths in the precast units are also shown. The main longitudinal bars are located at ordinates of 200 mm and 400 mm in Figure 12a and at 100 mm, 300 mm and 500 mm in Figure 12b. Crack widths are shown at a moment of 59 kNm which is 50% of the flexural yield load of B2-39-2H20-S-0. The only precast cracks captured by the DIC cameras were at the loading points which were around 200 mm from the joint-to-precast interfaces. Other flexural cracks were outside the field of view of the cameras.

Crack widths were greatest at the joint-to-slab interface in both the control and headed bar specimens. In Figure 12a, crack widths are very wide at the edge of the joint due to the large distance of 200 mm to the nearest continuous longitudinal bar. Consequently, the crack widths between and over the two H25 bars are most relevant to practice. Crack widths at the interface were least in the control specimen B1-39-/-/-/

with a width of 0.31 mm at the centre of the specimen. At the same location, crack widths were 0.37 mm in specimen B2-39-2H20-S-0 and up to 0.68 mm in specimens with lower concrete joint strengths. The comparison between B1-39-/-/-/ and B2-39-2H20-S-0 is most pertinent since the concrete strength and failure loads of both slabs were comparable. The crack widths within the precast planks were similar for all specimens, with an average of 0.20 mm. Precast plank crack widths for specimen B2-26-2H20-/-0 are not included as the planks were pre-cracked from previous testing.

Interface cracks in Figure 12b, on the three bar side, are generally lower than 0.40 mm, but up to 0.53 mm was observed for specimen B2-26-2H20-S-10 with the 10 mm vertical offset. Crack widths in the control specimen B1-39-/-/-/ are generally larger than in the headed bar specimens due to the smaller longitudinal bar area provided through the joint. Cracks in the precast planks for the headed bar specimens were typically around 0.10 mm wide on the three bar side.

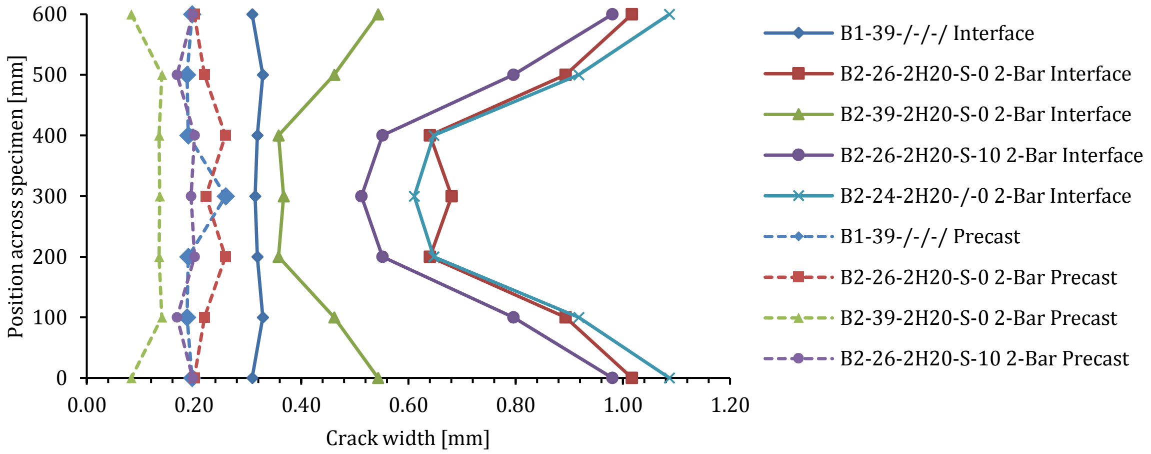

(a)

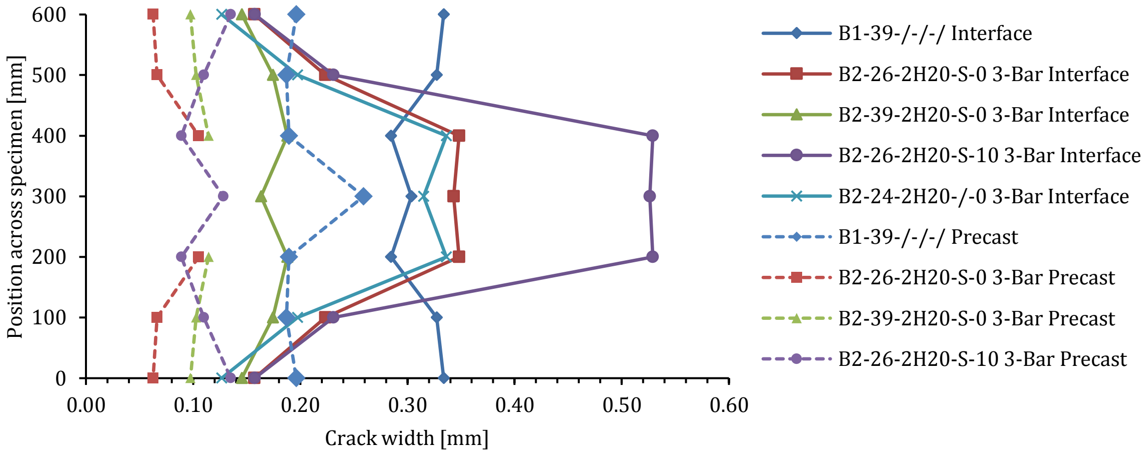

(b)

Figure 12: Crack widths at 59 kNm on a) two-bar side and b) three bar side

Removal of loose concrete immediately after testing revealed a failure mechanism wherein the headed bars slipped over the transverse bars with diagonal failure planes only evident up to the depth of the transverse bars. Figure 13 shows a photo of specimen B2-24-2H20-/-0 after two of the headed bars were cut at the interface and extracted with a wedge of concrete still attached to the head, and a corresponding sloping failure plane at the transverse bar. This mechanism is further facilitated by the offset joint since the transverse bars are not fully engaged within the overlapping head area of opposite headed bars. A similar failure mechanism was observed in the three bar tension tests [15].

Figure 13: Failure planes after removal of headed bars

3.3. Longitudinal joint reinforcement forces

The maximum tensile forces that developed in the longitudinal headed bars of the flexural splice were compared with those developed in comparable direct tension tests. The tensile force in the slab tests was back calculated from sectional analysis assuming plane sections remain plane. The 16 mm bars near the compression zone were included in the analysis. The following compressive stress strain relationship from EC2 [21] was used for concrete:

$$\sigma_c = f_{cm}\left(\frac{k\eta - \eta^2}{1+(k-2)\eta}\right) \qquad \text{for} \qquad 0 \leq \varepsilon_c \leq 3.5 \qquad (1)$$

where:

f_{cm} is the mean concrete cylinder strength, which is taken as the measured cylinder strength for the calculations in this paper,

$$\eta = \frac{\varepsilon_c}{\varepsilon_{c1}} \qquad (2)$$

$$\varepsilon_{c1} = 0.7{f_{cm}}^{0.31} \qquad (3)$$

$$k = 1.05E_{cm}\varepsilon_{c1}/f_{cm} \qquad (4)$$

$$E_{cm} = 22\left(\frac{f_{cm}}{10}\right)^{0.3} \tag{5}$$

ε_c is the strain in the compression zone concrete, ε_{c1} is the strain at peak compressive stress, and E_{cm} is the concrete elastic modulus.

Figure 14 shows the relationship between applied bending moment and longitudinal bar forces N_{hb} derived from strains adjacent to bar heads. On the three bar side, the edge bar force $N_{3hb,edge}$ was calculated from equilibrium as: $N_{3hb,edge} = N_{2hb} - 0.5N_{3hb,centre}$, where N_{2hb} is the bar force on the two bar side (gauges S1-S2 and S6-S7), and $N_{3hb,centre}$ is the force in the central bar on the three bar side (gauges S4-S5). Figure 14 shows that $N_{3hb,centre}$ is around N_{2hb} making forces in the edge bars $N_{3hb,edge}$ approximately $0.5N_{3hb,centre}$.

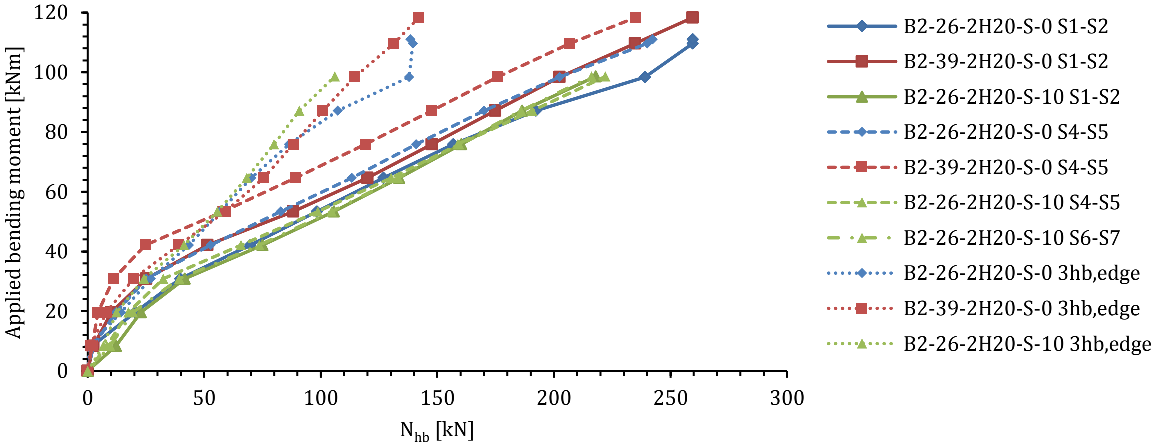

Figure 14: Longitudinal headed bar force comparisons

Figure 15, which is typical, compares bar forces in specimen B2-39-2H20-S-0 derived from section analysis (S.A.) and measured strains (see Figure 7a). Measured bar forces on the two-bar side (S1-S2) were similar to those calculated with section analysis, but forces on the three bar side (S4-S5 and 3hb,edge) are incorrectly calculated by section analysis to be equal.

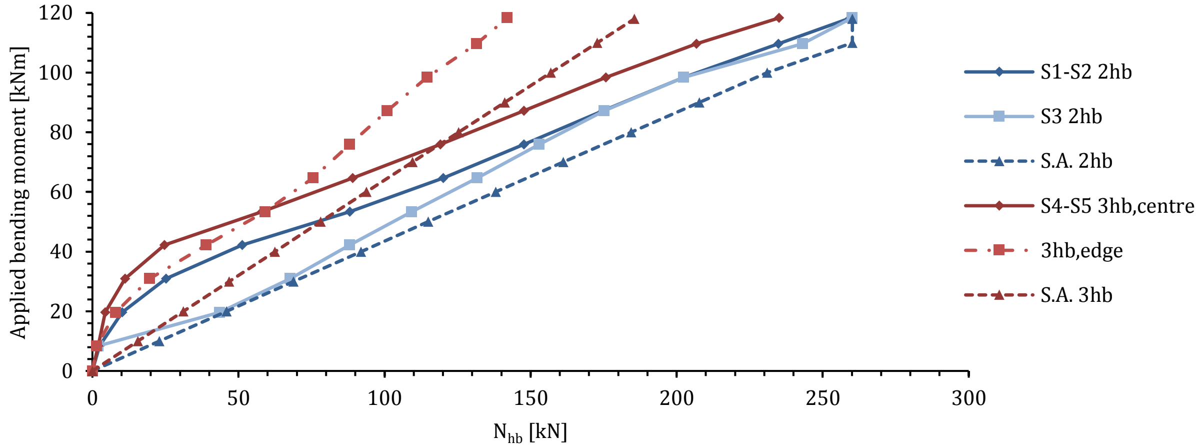

Figure 15: Specimen B2-39-2H20-S-0 longitudinal headed bar force comparisons to sectional analysis

Figure 16 shows the interaction between axial load and bending moment at the heads of longitudinal bars with the final point for each specimen corresponding to the least of the failure and measured yield loads. Bending moments are in the same sense as the applied moment with positive moments corresponding to maximum tensile strain within the cover zone. The forces are normalised by plastic capacities calculated using an idealised elastic-plastic stress-strain curve since the reinforcement had a well-defined yield plateau and measured strains did not approach the strain hardening region. Peak moments M_{hb} were below 10% of the bar plastic moment capacity $M_{p,hb}$ except for the misaligned specimen B2-26-2H20-S-10 in which M_{hb} reached 18% of $M_{p,hb}$. The bending moment in the headed bars on the two bar side (solid lines), which is critical, reduced to zero or near zero at peak N_{hb}.

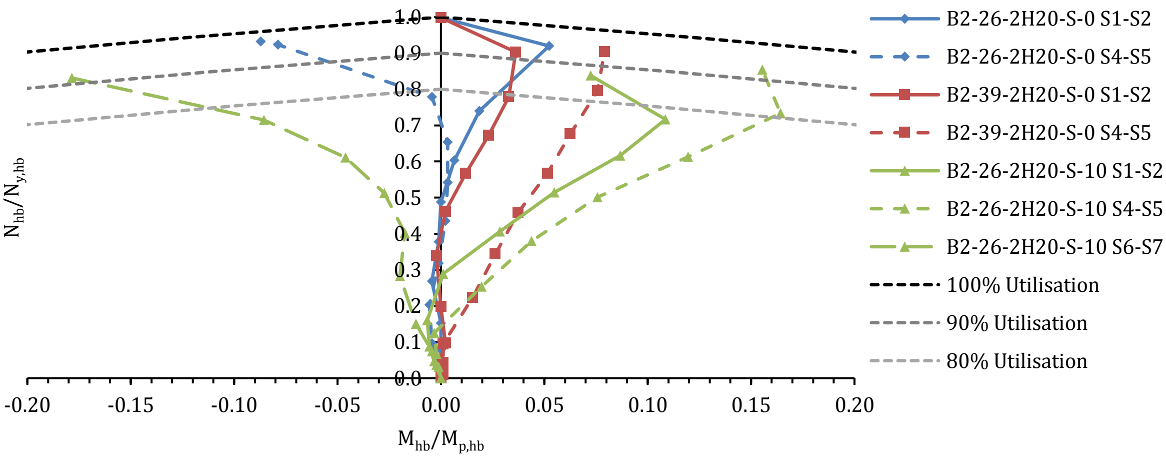

Figure 16: Longitudinal headed bar force interaction

3.4. Transverse Joint reinforcement forces

Figure 17 shows an axial load (N_{tr})-bending moment (M_{tr}) interaction diagram for the transverse bars with final points for each specimen corresponding to the least of the failure and measured yield loads. The plane of bending is horizontal with positive moment corresponding to maximum tension in gauges

S10, S12, S14 and S16 (see Figure 7a). Reversal of bending moments, due to continuous beam action, causes the change in sign visible in Figure 17 between gauges S9-S10 and S13-S14 as well as between gauges S11-S12 and S15-S16. At similar applied bending moments, forces in the transverse bars were lowest in specimen B2-39-2H20-S-0 with the highest joint concrete strength. Figure 17 shows that tension was greatest in the T' bar of Figure 7a (S9-S10, S13-S14) with the maximum force typically occurring at gauges S13-S14 midway between the edge and central bar on the three bar side. The tensile force in this bar was least at its end (S17) where the force was between 35-40% less than at gauges S13-S14. Bending moments were similar in the T and T' bars and proportionately greater in specimens with the least concrete strength. In no case was the full plastic capacity of the transverse bars achieved under combined axial and bending forces.

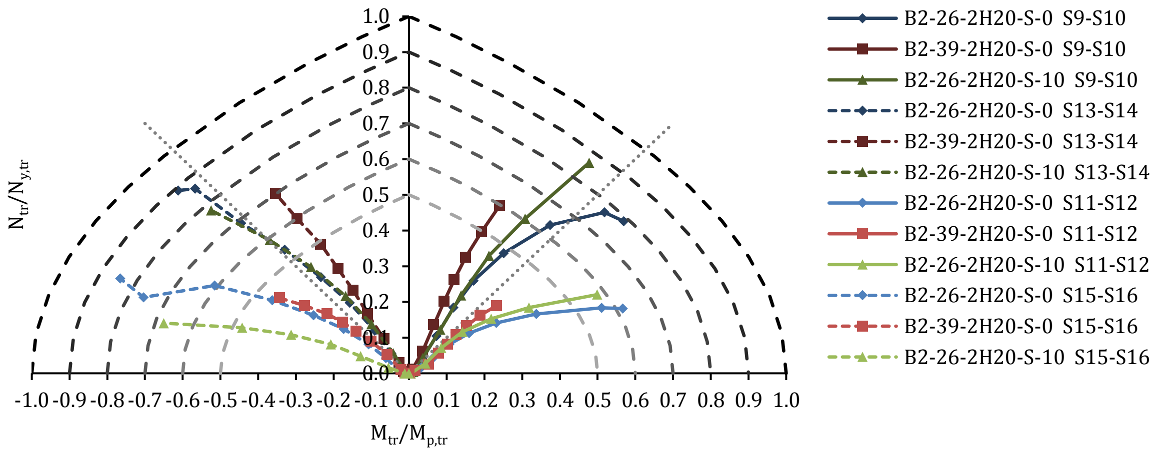

Figure 17: Transverse bar force interaction

Figure 18 and Figure 19 respectively compare the development with N_{hb} of transverse bar axial force N_{tr} and bending moment M_{tr} in the slab and tension tests. In the slab tests, the longitudinal bar force N_{hb} is calculated at gauges S1-S2 adjacent to the head on the two bar side. Transverse bar axial tension N_{tr} and bending moment M_{tr} are shown at gauges where strains were greatest. N_{tr} and M_{tr} increase more rapidly with load in tension specimens (dashed line) than comparable flexural specimens (solid line) probably due to transverse bending in the former. Up to near failure, axial tension at corresponding gauge positions is almost independent of concrete strength for both slab and tension specimens with tension greatest in T' bars (see Figure 7). Conversely, bending moments were similar in T and T' bars of both slab and tension specimens with moments increasing as the concrete strength reduced.

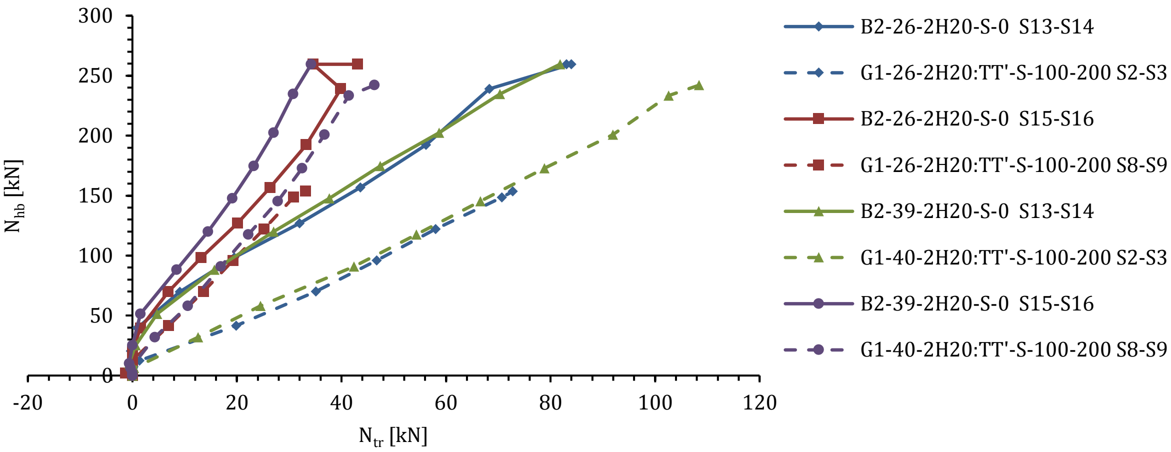

Figure 18: Transverse bar axial forces

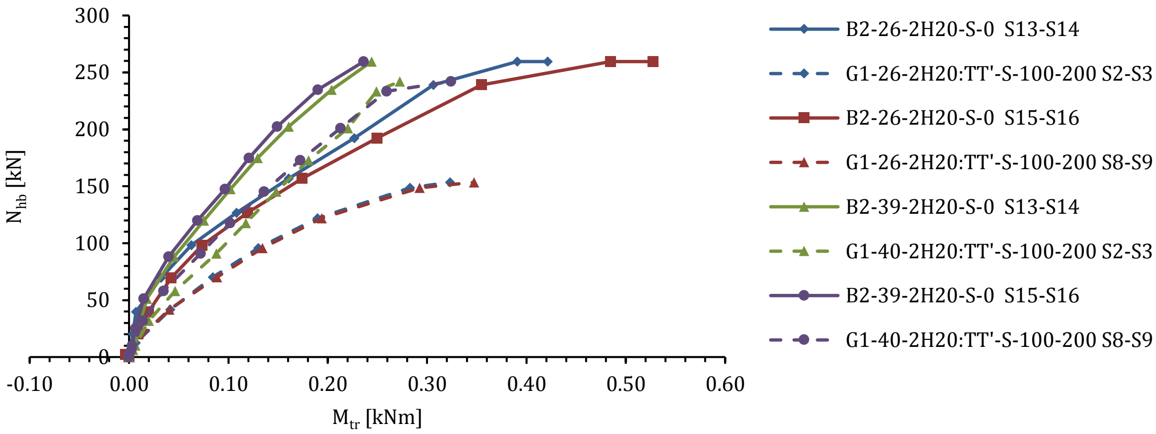

Figure 19: Transverse bar bending moments

3.5. Shear stud strains

Figure 20 compares the development with N_{hb} of strains in the shear studs of the slab and tension tests in which the stud diameters were 12 mm and 10 mm respectively. In the slab tests, N_{hb} is calculated at gauges S1-S2 adjacent to the head on the two bar side. Strains are always greater at gauge S19 than S20, suggesting out-of-plane confinement is greatest between highly stressed longitudinal bars. Up to near failure, strains were similar in aligned slab and tension specimens and fairly independent of concrete strength. Maximum strains did not exceed 65% of yield at ultimate strength except for the misaligned specimen in which yielding occurred at gauge S19. This suggests that the shear studs not only provide confinement to the joint concrete, but also balance out-of-plane forces arising from the transfer of force between the misaligned bars.

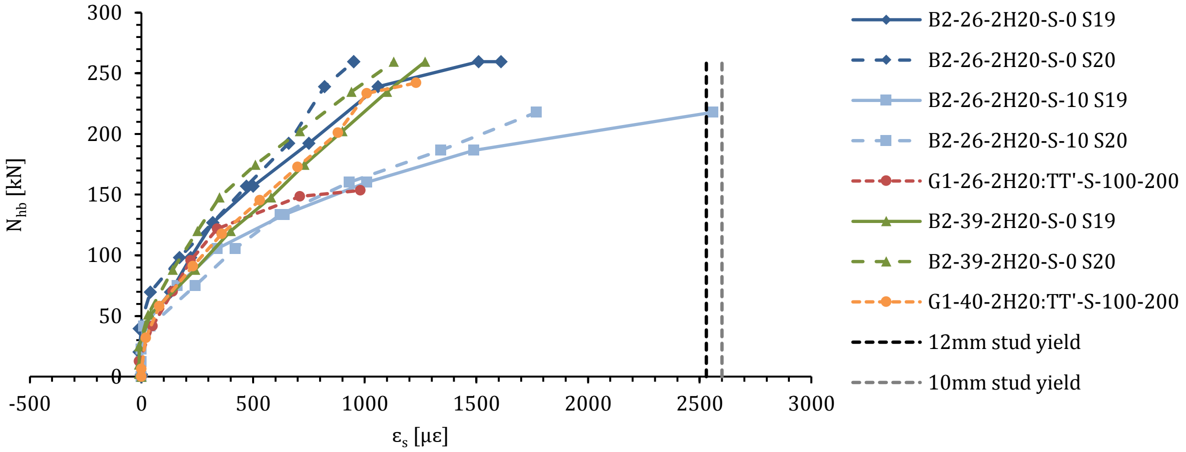

Figure 20: Shear stud axial strain

4. Numerical Modelling

As shown in this section, the flexural resistance of the joints was greater than calculated from the strength of comparable direct tension specimens. Furthermore, as discussed in Section 3.3, the central headed bar resisted twice the load of the edge bars contrary to the predictions of section analysis assuming plane sections remain plane. Therefore, NLFEA was carried out to determine whether it could explain these observations. The adopted NLFEA procedure has previously been shown to be capable of simulating the response of the three bar direct tension specimens [22]. The nonlinear finite element model (NLFEM) was developed with the package ATENA-GiD [23]. GiD was used for pre-processing, while analysis and post-processing were carried out in ATENA Studio [24].

4.1. Geometry and finite element mesh

To reduce computational requirements and exploit symmetry, only half of the joint region was modelled, omitting the precast sections. Furthermore, only the steel reinforcement in the tensile zone was modelled in full detail. Adopted model parameters were validated by NLFEA of the authors' tensile tests [22]. Quadratic 20-noded "CCIsoBrick" isoparametric brick elements with 27 gauss points were used for all the concrete and steel components except for shear studs and transverse bars near the compression zone where linear embedded "CCIsoTruss" truss elements were used. Bars in the tensile zone were modelled with brick elements with square cross-sections having the same second moment of area as the provided circular bars. Brick elements were needed to capture bending behaviour since 1D truss elements in ATENA only have axial stiffness [25]. The maximum element size was limited to 9 mm in the tensile zone of the specimen, producing nodes roughly every 4.5 mm along element edges. The ends of the headed bars were modelled with linear elastic 4-noded "CCIsoTetra" isoparametric tetrahedral elements, depicted loading plates, to avoid issues from stress concentrations. For simplicity, the heads of the shear studs were modelled entirely outside of the concrete and square (Figure 21a, b) with a similar surface area to the actual heads.

Perfect bond was assumed between reinforcement and concrete. Pryl and Cervenka [25] suggest this is realistic for ribbed bars provided the mesh size is comparable with the bar diameter as in the current analysis. Physical justification is provided by the reduction in stiffness of the concrete surrounding the reinforcement bar that arises due to localised cracking. Bearing faces of bar heads were connected to the concrete using "fixed contacts" consisting of master-slave constraints as shown in Figure 21c. None of the other bar head faces were connected to the concrete. Fixed contacts were also required at interfaces between loading plates and longitudinal bars, due to differences in element type, as well as between steel and concrete at the bearing faces of shear stud heads.

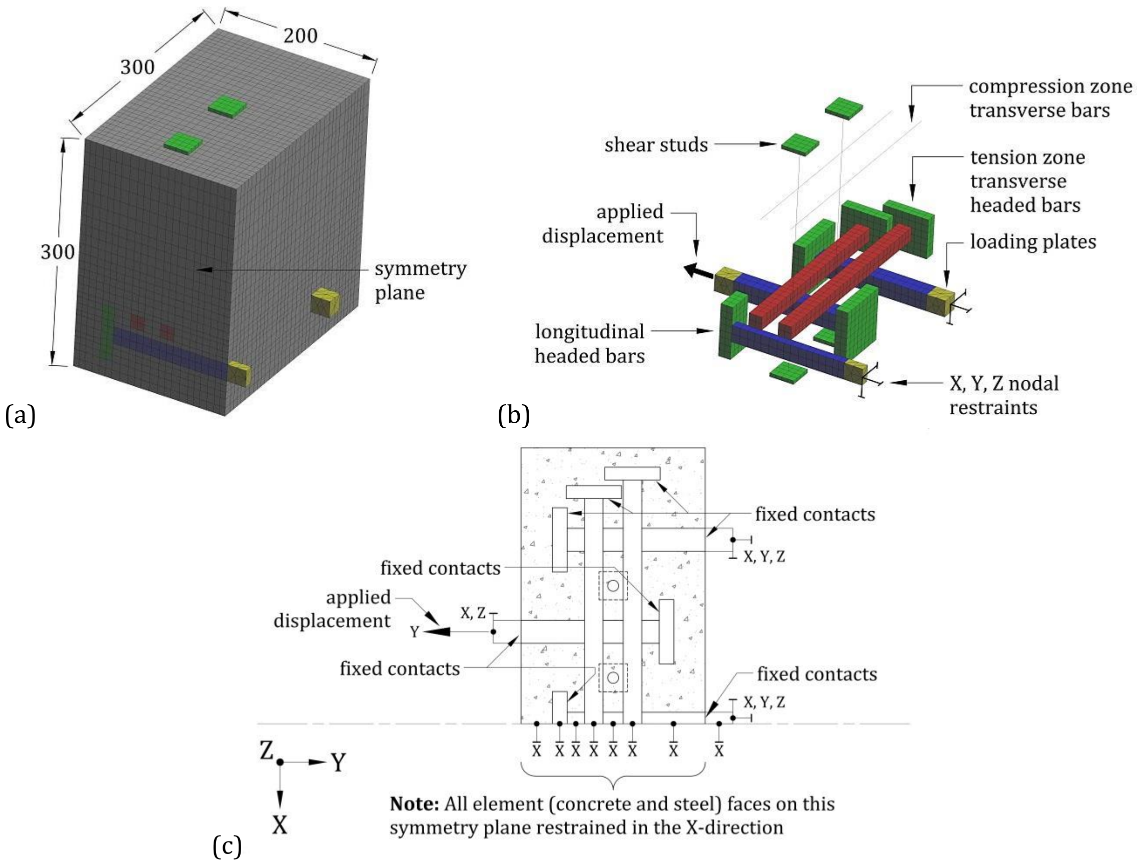

Figure 21: Full NLFEM (a) NLFEM steel components only (b) and Boundary conditions (c)

4.2. Boundary conditions

The boundary conditions applied to the model are shown in Figure 21c. The central node of the end faces of the loading plates of the supporting bars were constrained in all directions. A prescribed displacement of 0.0125 mm per load step was applied in the negative y-direction at the central node of the end plate of the loaded bar, which was also restrained vertically in the z-direction. End displacements were monitored at the end of this bar, on the inside face of the loading plate. All element faces on the plane of symmetry were restrained in the x-direction.

4.3. Material constitutive models

Concrete was modelled in ATENA with "CC3DNonLinCementitious2" which is a smeared crack fracture-plastic model that combines constitutive models for tensile and compressive behaviour. The fixed crack option of ATENA with variable shear retention factor was chosen on the basis of sensitivity studies for the three bar tension specimens [22]. Concrete material parameters were automatically generated in ATENA-GiD in terms of the mean measured concrete cylinder compressive strength and then modified as shown in Table 4 which summarises key material parameters used in the analysis. The parameters w_d and r_c were derived from sensitivity studies on three bar tension specimens [22]. Transverse and longitudinal bars and heads in the tensile zone were modelled using the "CC3DBiLinearSteelVonMises" material model which has a bilinear elastic-plastic stress-strain law. The perfectly elastic material "CC3DElastIsotropic" was used for the loading plates at the ends of the longitudinal headed bars. The shear studs and transverse bars near the compression zone were modelled as "CCReinforcement". A trilinear elastic-plastic stress strain relationship was used for the shear studs, while a bilinear law was used for the transverse bars for consistency with those in the tension zone. Adopted steel material properties are given in Table 5 and Table 6. More information on the material constitutive models can be found in reference [26].

Parameter	Function	
Cylinder strength	f'_c = Measured (given in Table 2)	
Tensile strength	f'_t = Measured (given in Table 2)	
Compression softening	w_d = -1.8 mm	
Compressive strength in cracked concrete	r_c = 0.3	
Onset of nonlinear behaviour	$f'_{c0} = 2f'_t$	(Default function)
Fracture energy	$G_f = 73f_{cm}^{0.18}$	(Default value)
Shear factor	S_F = 20	(Default value)
Maximum aggregate size	d_g = 10 mm	

Table 4: ATENA concrete constitutive model parameters

Component	E_s (GPa)	σ_y (MPa)	H (MPa)	ν
Bar heads	200	355	1.0e+4	0.3
25 mm headed bars	197	530	1.0e+4	0.3
20 mm headed bars	201	516	1.0e+4	0.3
Loading Plate	2.0e+4	—	—	0.05

Table 5: ATENA 3D steel material properties

Component	E_s (GPa)	σ_y (MPa)	ε_2	σ_2 (MPa)	ε_3	σ_3 (MPa)
20 mm compression headed bars	201	516	0.040	890	—	—
12 mm shear studs	223	564	0.026	564	0.060	637

Table 6: ATENA 1D reinforcement material properties

5. Numerical Modelling Results and Discussion

The predicted and observed crack patterns and surface principal tensile strains compare well as shown in Figure 9 for specimen B2-26-2H20-S-0. As developed, the NLFEM does not allow comparison of measured and predicted interface crack widths.

Table 7 shows measured and predicted failure loads P for the tested slabs and corresponding joint-to-precast interface bending moments M. Equivalent results are also given for the corresponding tension specimens for which the measured failure loads N_{2hb} are similar to bar forces at the bar head [15] derived from strains. The values of M and P for tension specimens were derived from N_{2hb} using section analysis and equilibrium respectively. Table 7 also shows corresponding "measured" individual bar forces on the two and three bar sides of the joint denoted N_{2hb}, $N_{3hb,centre}$ and $N_{3hb,edge}$. The measured slab test bar forces N_{2hb} and $N_{3hb,centre}$ were derived from strains measured adjacent to the bar head while $N_{3hb,edge}$ was calculated from equilibrium as $N_{3hb,edge} = N_{2hb} - 0.5N_{3hb,centre}$.

Test ID	Specimen type	P (kN)	M (kNm)	N_{2hb} (kN)	$N_{3hb,centre}$ (kN)	$N_{3hb,edge}$ (kN)
B2-26-2H20-S-0 (test)	Slab	253	111	260	242	139
B2-26-2H20-S-0 NLFEA	Slab	211	95	211	206	108
G1-26-2H20:TT-S-100-200 (test)	Tension	171	74	154	–	–
G1-26-2H20:TT-S-100-200 NLFEA	Tension	197	86	187	–	–
B2-39-2H20-S-0 (test)	Slab	293	129	260	235	143
B2-39-2H20-S-0 NLFEA	Slab	260	121	260	253	134
G1-40-2H20:TT-S-100-200 (test)	Tension	260	114	242	–	–
G1-40-2H20:TT-S-100-200 NLFEA	Tension	251	110	232	–	–
B2-24-2H20-/-0 (test)	Slab	192	84	–	–	–
B2-24-2H20-/-0 NLFEA	Slab	179	82	179	170	94
G2-26-2H20:TT-100-200 (test)	Tension	153	66	133	–	–
G2-26-2H20:TT-100-200 NLFEA	Tension	175	76	159	–	–
B2-26-2H20-S-10 (test)	Slab	225	99	218	222	107
B2-26-2H20-S-10 NLFEA	Slab	187	81	187	173	101

Table 7: Test specimen capacities and longitudinal bar axial forces

The slab NLFEA longitudinal headed bar forces in Table 7 are reactions at the end of the bars (X, Y, Z nodal restraints shown in Figure 21b), rather than internal forces at the head as measured in the tests. The NLFEA closely predicts the observed distribution of load between the centre and edge bars, with edge bars resisting approximately half the force in the central bar unlike section analysis which predicts equal forces in all three bars. As observed, the NLFEA also predicts lower strengths N_{hb} for tension than flexural tests though prying action is not modelled in the latter. The capacity of the tension specimens is thought to be reduced by bending in the plane of loading being more severe than in the longer slab joints.

Figure 22 shows that the flexural resistances derived from the tension tests broadly follow the trend of the measured slab flexural resistances giving added confidence that it is safe to base the flexural design strength of headed bar splices, of the tested geometry, on three bar tension tests of the type undertaken.

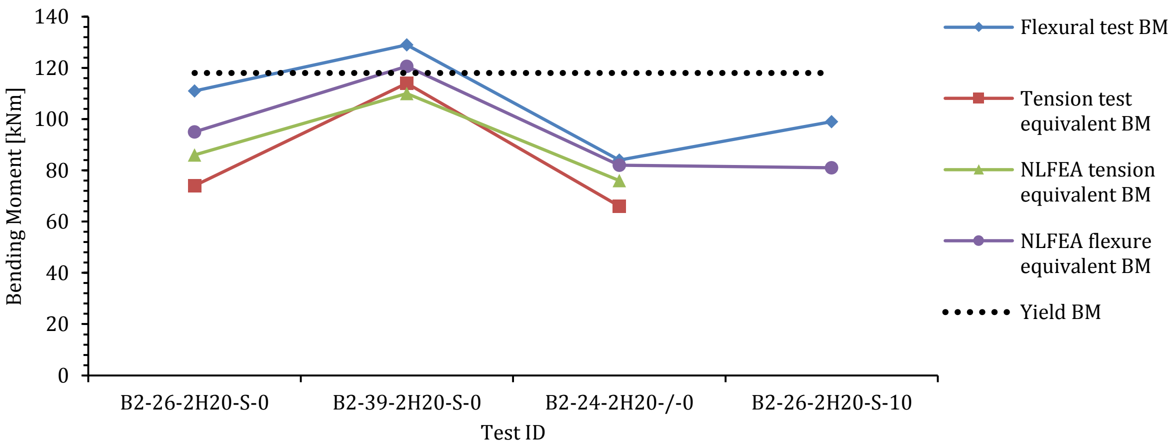

Figure 22: Comparison between test and NLFEA results

Figure 23 and Figure 24 compare transverse bar forces derived from strain gauge readings and NLFEA at the cross-over with the central longitudinal headed bar. Transverse bar forces are plotted against the force in the central longitudinal headed bar. The numerical results follow the trends of the test data relatively well, but the measured forces are generally underestimated.

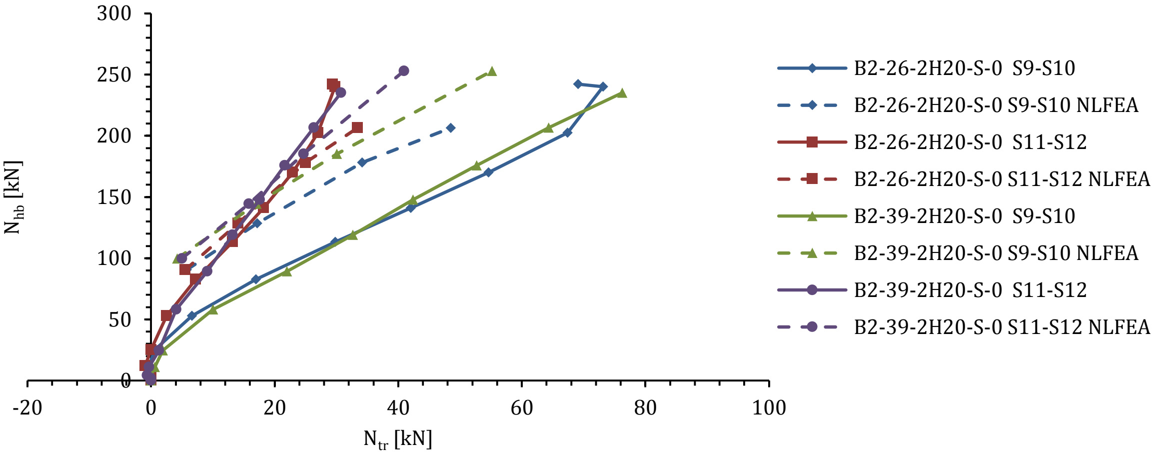

Figure 23: Comparison between measured and NLFEA transverse bar axial forces

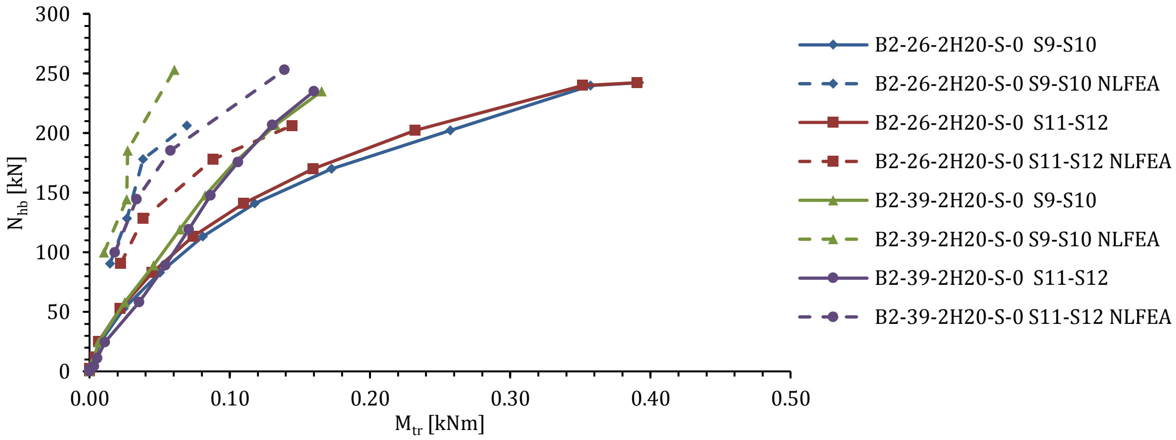

Figure 24: Comparison between measured and NLFEA transverse bar bending moments

Figure 25 compares measured and predicted forces in the shear studs. As with transverse bar forces, the NLFEA captures the general trend of behaviour but underestimates measured forces. The underestimate of stud force may result from the absence of prying action in the NLFEA since only tension is applied in the model.

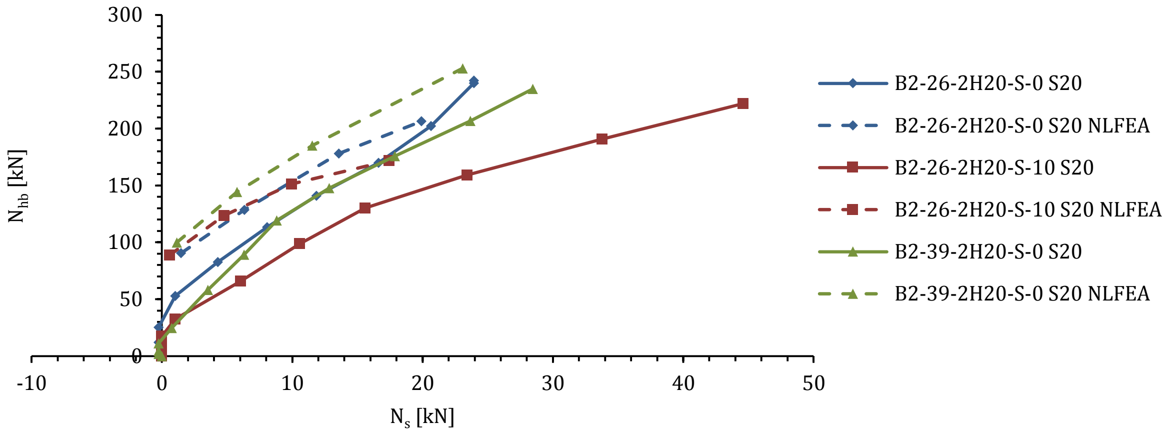

Figure 25: Comparison between measured and NLFEA shear stud axial forces

6. Conclusions

The paper describes a series of flexural tests on precast concrete slabs connected by headed bar splices. This type of connection facilitates precast concrete construction thereby increasing construction efficiency due to significantly reduced on-site work. The tests investigated the influence on slab strength and stiffness of joint concrete strength, shear studs, and out-of-plane offset of precast planks. Lap strengths are compared with strengths of comparable direct tension splices previously tested by the authors as part of the same project. NLFEA of these joints with ATENA-GiD captures the overall joint behaviour reasonably well and gives good estimates of flexural strength. The NLFEM is considered suitable for the design of standard joint configurations provided a suitable safety format is adopted. Alternatively, the splice strength can be calculated using STM [15] or the upper bound plasticity model of Joergensen and Hoang [13] as presented in [15].

Key conclusions from the tests are:

a) A lap length of 100 mm in 39 MPa joint concrete was found sufficient to develop the full yield strength of H25 headed bars when detailed with confining reinforcement as shown in Figure 4. Ductility was comparable to that of the control specimen with continuous reinforcement through the joint.

b) Small scale tension tests give a good indication of joint behaviour and conservative predictions of flexural strength.

c) Flexural strength and stiffness is mainly affected by joint concrete strength.

d) Vertical out-of-plane offset within the joint does not significantly reduce flexural strength.

e) Shear studs increase joint strength by providing confinement to the joint concrete and restraining prying action of the headed bars in flexural specimens. Shear studs also balance any out-of-plane stresses arising due to construction tolerances.

f) Precast-to-joint interface crack widths reduce with increasing joint concrete strength but appear to be within acceptable limits at the serviceability limit state as defined in EC2.

The understanding of joint behaviour at both ultimate and serviceability limit state gained in this research gives better confidence for a more widespread use of headed bar splices in precast concrete construction.

7. Acknowledgements

This is a research project funded by Laing O'Rourke. The authors would like to thank Arup for their collaboration in this project. Thanks also to the technicians at the Structures Laboratory at Imperial College London, in particular Mr. Leslie Clark and Mr. Stefan Algar for their availability and assistance throughout the testing programme.

References

1. Chun, S.C., *Lap Splice Tests Using High-Strength Headed Bars of 550 MPa (80 ksi) Yield Strength.* ACI Structural Journal, 2015. **112**(6): p. 679 - 688.
2. Li, L., Ma, Z., Griffey, M.E., and Oesterle, R.G., *Improved Longitudinal Joint Details in Decked Bulb Tees for Accelerated Bridge Construction: Concept Development.* Journal of Bridge Engineering, 2010. **15**(3): p. 327-336.
3. Li, L., Ma, Z., and Oesterle, R.G., *Improved Longitudinal Joint Details in Decked Bulb Tees for Accelerated Bridge Construction: Fatigue Evaluation.* Journal of Bridge Engineering, 2010. **15**(5): p. 511-522.
4. Li, L. and Jiang, Z., *Flexural Behavior and Strut-and-tie Model of Joints with headed bar details Connecting Precast Members.* Perspectives in Science, 2016. **7**: p. 253-260.
5. Thompson, M.K., Jirsa, J.O., and Breen, J.E., *Behaviour and Capacity of Headed Reinforcement.* ACI Structural Journal, 2006. **103**(4): p. 522-530.

6. Thompson, M.K., Ledesma, A., Jirsa, J.O., and Breen, J.E., *Lap Splices Anchored by Headed Bars.* ACI Structural Journal, 2006. **103**(2): p. 271-279.

7. Gordon, S.R. and May, I.M., *Development of In-situ Joints for Pre-cast Bridge Deck Units.* Proceedings of the Institution of Civil Engineers: Bridge Engineering, 2006. **159**(BE1): p. 17-30.

8. Gordon, S.R. and May, I.M., *Precast Deck Systems for Steel-Concrete Composite Bridges.* Proceedings of the Institution of Civil Engineers: Bridge Engineering, 2007. **160**(BE1): p. 25-35.

9. He, Z., Ma, Z.J., Chapman, C.E., and Liu, Z., *Longitudinal Joints with Accelerated Construction Features in Decked Bulb-Tee Girder Bridges: Strut-and-Tie Model and Design Guidelines.* Journal of Bridge Engineering, 2013. **18**(5): p. 372-379.

10. Ong, K.C.G., Hao, J.B., and Paramasivam, P., *A Strut-and-Tie Model for Ultimate Loads of Precast Concrete Joints with Loop Connections in Tension.* Construction and Building Materials, 2005. **20**(3): p. 169-176.

11. Ma, Z.J., Lewis, S., Cao, Q., He, Z., Burdette, E.G., and French, C.E.W., *Transverse Joint Details with Tight Bend Diameter U-Bars for Accelerated Bridge Construction.* Journal of Structural Engineering, 2012. **138**(6): p. 697-707.

12. Joergensen, H.B. and Hoang, L.C., *Tests and Limit Analysis of Loop Connections between Precast Concrete Elements Loaded in Tension.* Engineering Structures, 2013. **52**: p. 558-569.

13. Joergensen, H.B. and Hoang, L.C., *Strength of Loop Connections between Precast Bridge Decks Loaded in Combined Tension and Bending.* Structural Engineering International, 2015. **25**(1): p. 71-80.

14. ACI, *Building Code Requirements for Structural Concrete (ACI 318-02) and Commentary (ACI 318R-02)*. 2002, American Concrete Institute Committee 318. p. 443.

15. Vella, J.P., Vollum, R.L., and Jackson, A., *Investigation of Headed Bar Joints between Precast Concrete Panels.* Engineering Structures, 2017. **138C**: p. 351-366.

16. Brooker, O., *Use of Headed Bars as Anchorage to Reinforcement.* The Structural Engineer, 2013: p. 49-57.

17. BSI, *Testing hardened concrete Part 3: Compressive strength of test specimens*. 2009, British Standards Institution. p. 22.

18. BSI, *Testing hardened concrete Part 6: Tensile splitting strength of test specimens*. 2009, British Standards Institution. p. 14.

19. BSI, *Metallic materials - Tensile testing - Part 1: Method of test at room temperature*. 2009, British Standards Institution. p. 76.

20. LaVision, *Product Manual for DaVis 8.3*. 2016, LaVision GmbH: Gottingen, Germany. p. 356.

21. BSI, *Eurocode 2: Design of concrete Structures - Part 1-1: General Rules and Rules for Buildings*. 2004, British Standards Institution. p. 225.

22. Vella, J.P., Vollum, R.L., and Jackson, A., *Numerical Modelling of Headed Bar Joints subjected to Tension.* Magazine of Concrete Research, 2017. DOI: 10.1680/jmacr.17.00011.

23. Cervenka, V., Cervenka, J., Janda, Z., and Pryl, D., *ATENA Program Documentation, Part 8: User's Manual for ATENA-GiD Interface*. 2014, Cervenka Consulting: Prague. p. 112.

24. Benes, S., Mikolaskova, J., and Altman, T., *ATENA Program Documentation, Part 12: User's Manual for ATENA Studio*. 2015, Cervenka Consulting: Prague. p. 58.

25. Pryl, D. and Cervenka, J., *ATENA Program Documentation, Part 11: Troubleshooting Manual*. 2014, Cervenka Consulting: Prague. p. 51.

26. Cervenka, V., Jendele, L., and Cervenka, J., *ATENA Program Documentation, Part 1: Theory*. 2013, Cervenka Consulting: Prague. p. 268.